UDC 551.576.11:551.571.7:551.511.33.001.57

HUMIDITY AUGMENTATION AS THE INITIAL IMPULSE IN A NUMERICAL CLOUD MODEL

F. W. MURRAY
The Rand Corporation, Santa Monica, Calif.

ABSTRACT

A perturbation of relative humidity is used as a trigger to start the convection in a two-dimensional numerical model of a cumulus cloud. The effects of varying the width and depth of the perturbation are studied. The rate of growth, eventual cloud height, liquid water content, and updraft strength are strongly dependent on depth of the impulse; but for realistically shallow depths, these values are in reasonable agreement with observations of real clouds. As in the case of one-dimensional models, the ultimate cloud height is dependent on the width of the impulse, but perhaps to a lesser extent.

1. INTRODUCTION

Following the pioneering work of Malkus and Witt (1959) and Ogura (1963), many scientists have created a proliferation of models for numerical simulation of cumulus convection by solution in two dimensions of the equations of hydrodynamics and thermodynamics. Many one-dimensional models also have been created, based on the assumption of a specified form such as a plume or a spherical vortex and involving extensive parameterization. A presumed advantage of the two-dimensional model is that, since no form and few arbitrary parameters need be specified, the characteristics of the simulated cloud should depend more on the physics behind the basic equations, which are universal in application, than on the investigator's preconceived notion of the phenomenon he is modeling.

Unfortunately, the two-dimensional thermohydrodynamic models are not entirely free of arbitrary specifications. One example is eddy diffusion. Many of the models require an explicit eddy diffusion term for computational stability. Some have differencing schemes that introduce sufficient implicit eddy diffusion for this purpose; but even in these cases, it is often desirable to include an explicit term, which in turn requires a choice of a coefficient. But as Lilly (1962) has shown, determination of a suitable coefficient requires knowledge of some quantities that cannot be observed well. Fortunately, the magnitude of the coefficient is not critical over about an order of magnitude, and there is some physical basis for choice. A value of 40 $m^2\ s^{-1}$ was favored by Ogura (1963) and Orville (1968); the same value was used in the present study.

Another important arbitrary specification for this type of model is that of the initial impulse, and here we come close to the preconception of form that is basic to the one-dimensional model. Hence, we should exercise a great deal of care in its choice. The usual practice is to assume that initially there is no motion and all variables are horizontally uniform except for some small perturbation that is introduced to initiate convection. It has generally been tacitly assumed that a sufficiently small perturbation by itself would not affect the later development to any significant degree, but there apparently has been no investigation to determine what constitutes a "sufficiently small" perturbation.

The perturbation may be thought of not only in mathematical terms but also in physical terms. Where there are obvious irregularities in terrain or sources of local heating, there is no difficulty in recognizing the perturbation in nature or in modeling it on a computer. But by and large, a tropical maritime atmosphere is uniform in the horizontal; yet, scattered cumuli develop throughout it. Obviously, such an atmosphere must have some small-scale irregularities that determine the initiation of a convective cell here but not there.

In most numerical models, the perturbation takes the form of an increase in temperature, usually not exceeding 1°C and usually confined to a region of horizontal and vertical dimension of 1 km or less. This perturbation supposedly simulates a thermal resulting from solar heating. One disadvantage of this approach in the study of moist convection is that, in the region where the temperature is arbitrarily increased, the relative humidity is correspondingly decreased. Yet, if the convection so initiated is to sustain itself and grow, condensation and release of latent heat must occur, and the lower humidity makes that development all the more difficult. One is faced with the anomalous situation of trying to grow a simulated cloud in the region of lowest humidity (as regards horizontal variation), whereas the physical process generally envisioned for the growth of tropical cumuli is that a series of small convective cells carry moisture aloft into a relatively dry level, each conditioning the air in that limited horizontal region for more vigorous development of the next cell.

A way out of this dilemma is to specify an initial perturbation of relative humidity rather than of temperature. If, in a limited region, the relative humidity is increased, a horizontal gradient of virtual temperature will result even though the actual temperature remains uniform in the horizontal. But since air density depends on virtual temperature rather than on actual temperature alone, the region with enhanced relative humidity is now more buoyant than its environment. Thus convection can

be initiated without the inhibiting effect of arbitrarily depressed humidity.

There is observational evidence for humidity variations of this type, but few quantitative reports are available for use in the present context. Vul'fson (1964) cites measurements by instrumented aircraft over the Black Sea that show ascending air currents to be initiated by horizontal gradients of humidity when temperature is uniform in the horizontal. He indicates deviations of dew point of over 2°C where the temperature varies no more than 0.1°C, but he does not specify the dimensions of the perturbed region.

Several more extensive sets of observations were carried out earlier over the Caribbean Sea by the Woods Hole Oceanographic Institution (Langwell 1948, Bunker et al. 1949, Malkus 1958); and though most of their published tabulations relate to variations in the vertical, there is also some information on variations in the horizontal, from which valuable guidance can be obtained. It is of interest to note that Langwell observed that mixing ratio and temperature are correlated in such a way that virtual temperature is more constant than actual temperature. Hence, those variations that occur in virtual temperature should represent relatively well-organized atmospheric systems rather than random fluctuations.

The arbitrary addition of moisture to the atmosphere is equivalent to the addition of energy to the system, and care must be taken that the energy so added is not so great as to mask the energy conversions that take place during the convection. The present study is meant to give some indication of the effects of humidity perturbations of different sizes and shapes; and in some respects, the perturbations used do not fulfill this requirement. Some of the test cases, however, are sufficiently close to realistic conditions to permit meaningful comparison of simulated clouds with real ones. Limitations of time and of observational data preclude an exhaustive study of this type, but it is believed that enough information has been obtained to give some useful insights and guidelines for further work in the numerical modeling of tropical cumulus convection.

2. THE MODEL

The model used in the present study, an outgrowth of the model of Murray and Anderson (1965), is similar to that of Ogura (1963), regarding computation of the field of motion; but temperature and moisture are handled in an entirely different manner. The derivation of the equations and a description of the method of their solution have been given by Murray (1970) and will not be repeated here. Briefly, axial symmetry and the Boussinesq approximation are assumed, leading to a vorticity equation of the form

$$\frac{\partial \eta}{\partial t}=-\left[\frac{\partial}{\partial r}(u\eta)+\frac{\partial}{\partial z}(w\eta)\right]-g\frac{\partial}{\partial r}\left[\frac{T^{*\prime}}{\overline{T^*}}-q_l\right]+\nu_M\left[\frac{\partial}{\partial r}\left\{\frac{1}{r}\frac{\partial}{\partial r}(r\eta)\right\}+\frac{\partial^2\eta}{\partial z^2}\right]$$

where t is time, r and z are the radial and vertical coordinates, u and w are the radial and vertical components of wind, η is the tangential component of vorticity, g is the acceleration due to gravity, $T^{*\prime}$ is the departure of virtual temperature from its basic value for the level, $\overline{T^*}$ is the mean virtual temperature over the whole region at time zero, q_l is the mixing ratio of liquid water, and ν_M is the coefficient of eddy transport of momentum. The vorticity equation is solved at each grid point, and relaxation is used to recover the stream function from the vorticity. All boundaries are considered to be rigid surfaces with free slippage along them.

Temperature and mixing ratios of water vapor and liquid water are computed in the Lagrangian sense, using a single-time-step backward trajectory and allowing for condensation and evaporation, but not for precipitation of the condensate. In the present series, the grid consisted of 30 points in the horizontal and 36 points in the vertical, with a mesh length of 200 m. Because of symmetry, this corresponds to a computational region about 12 km in diameter and 7 km in depth. In the four cases discussed here, the simulated cloud never came near the lateral boundary. In two cases, it approached the upper boundary; realism could not be expected after that time. In the other two cases, the maximum cloud top was well below the upper boundary.

The basic state was one of horizontal homogeneity of all variables, no motion, and no liquid water. The impulse consisted of an increase of mixing ratio (and consequently of relative humidity and virtual temperature) applied to a limited region. Presumably, for a given basic sounding, there is a smallest perturbation that can release the latent instability. In the present study, this smallest perturbation was neither sought nor discovered; instead, the perturbations were designed to simulate local conditions occurring immediately before the onset of condensation, and so they tend to be larger in magnitude than what one is likely to observe in horizontal flight through clear air, though not unreasonably so. For instance, typical observations published by Bunker et al. (1949) show regions of about 2 km in diameter with a mixing ratio 2 g kg^{-1} higher than the background value. In the present study, an increase of up to 4 g kg^{-1} is specified on the central axis, this being the amount required to bring the air up to saturation.

The vertical variation of the impulse is open to more question. In the present study, on the central axis a saturated layer 200–400 m in depth was specified near the lifting condensation level; this corresponds with the transition layer described by Bunker et al. (1949) and Malkus (1958) as typical of the Caribbean atmosphere. Below this layer, down to the surface of the sea, the mixing ratio was held constant, as in the mixed layer described by the same authors.

Above the transition layer up to 1500 or 2500 m, the mixing ratio fell off gradually to its ambient value; this corresponds to the cloud layer of the Woods Hole studies. The resulting perturbation for four cases is shown in figure 1. Unfortunately, the basic sounding, which is for San Juan, Puerto Rico, at 1200 GMT on July 17, 1967, did not conform

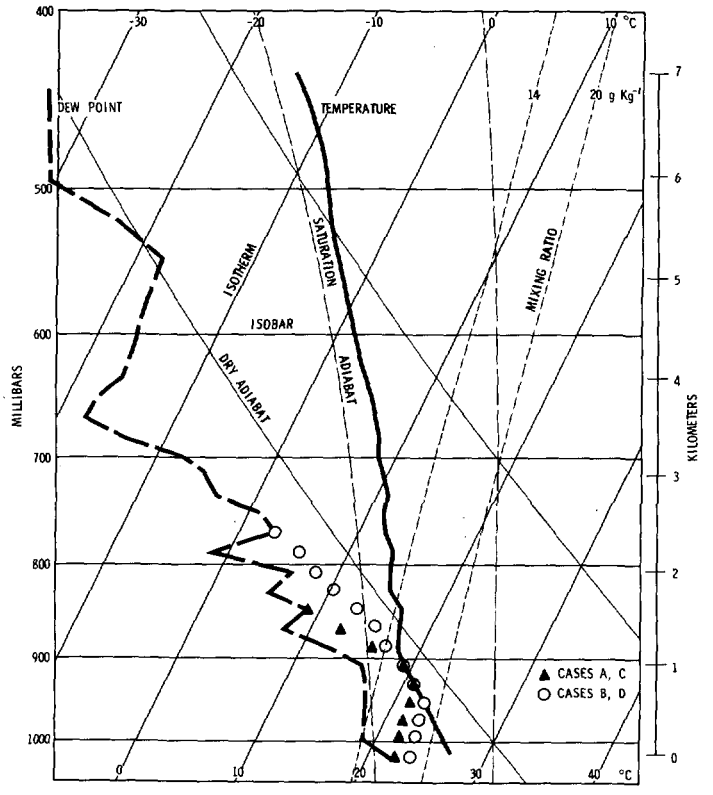

FIGURE 1.—Basic sounding for San Juan, Puerto Rico, at 1200 GMT on July 17, 1967. The perturbed humidity values on the central axis are indicated by triangles and circles.

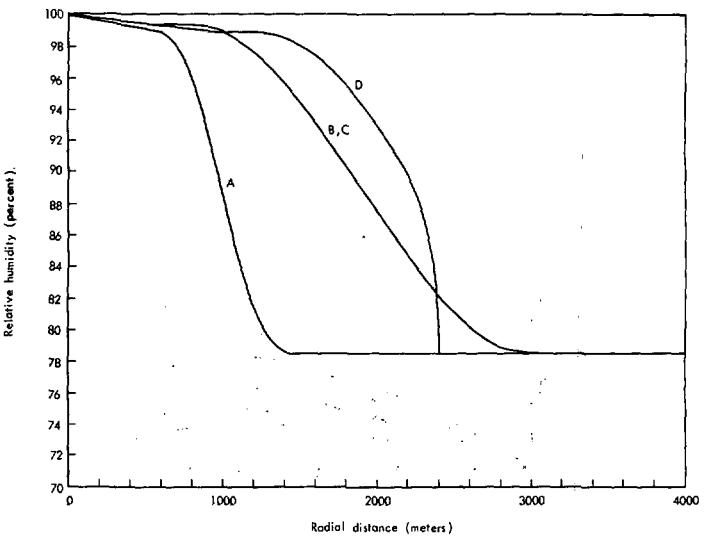

FIGURE 2.—Initial perturbation of humidity at a 1-km elevation.

TABLE 1.—*Characteristics of impulses*

Case	Depth	Width	Slope	Mass of water in perturbed region (kg)	
				Total before perturbation	Amount added
A	Shallow	Narrow	Steep	1.67×10^{8}	1.62×10^{7}
B	Deep	Wide	Gentle	8.53×10^{8}	1.08×10^{8}
C	Shallow	Wide	Gentle	7.13×10^{8}	6.14×10^{7}
D	Deep	Wide	Steep	5.55×10^{8}	1.26×10^{8}

well to the Caribbean models of Bunker and Malkus, with the result that there is a considerable boost in humidity over a rather deep layer. Observations in the Caribbean do not show this type of variation to occur; and so in that respect, the impulses used in the present study are not realistic, particularly for cases B and D. A case in which the disturbance was restricted to the transition layer has been discussed by Murray (1970); it did not display the excess development noted here in cases B and D.

In the horizontal, the impulse was assumed to diminish from its specified value on the central axis to zero at a radial distance of 1 to 3 km. The shape and width of the disturbance in four cases is shown in figure 2. The simulated cloud that results is invariably narrower than the initial perturbaton; hence a radius of 3 km for the perturbation is not excessive.

Two of the cases represent shallow impulses; and two cases, deep ones. One represents a narrow impulse; two represent wide ones with a gentle slope; and one represents a wide one with a steep slope. These characteristics are summarized in table 1. Also shown in table 1 is the total amount of water added to the system by the impulse and the total amount originally present in the volume covered by the perturbation. The total mass of water in the entire computational volume is 3.77×10^{9} kg. Rather large masses of water are involved; but except for case D, the amount of water vapor added is an order of magnitude less than that initially present in the corresponding volume. Impulses of this magnitude probably do not represent realistic natural variations in the atmosphere, and they certainly do not represent any feasible artificial modification; nevertheless, they are useful to test the response of the numerical model.

3. COMPARISON OF FOUR DIFFERENT IMPULSES

Although one of the most important advantages of a two-dimensional model is that it takes into account both horizontal and vertical variations in the cloud and its environment, it is frequently desirable to study some phases of the evolution of a two-dimensional simulated cloud by looking only at its central axis. Values here tend to be extreme and to epitomize the cloud as a whole.

Two particularly significant values are the vertical wind speed and the amount of liquid water. The first of these is illustrated in figures 3–6, and the second in figures 7–10. All of these figures are time sections of the distribution of the variable on the central axis. In all cases, the early development is characterized by regular increases in maximum updraft, height at which the updraft is a maximum, maximum amount of liquid water, and height of cloud top. All of these variables achieved their greatest value about the same time for a given case, but the timing and magnitudes were different in different cases.

The two deep-impulse cases showed strong and rapid development until the cloud top reached the upper boundary. At that time, the maximum updraft was 28 m s^{-1} in case B and 25 m s^{-1} in case D, rather unreasonable values. Computation for case B was terminated at that

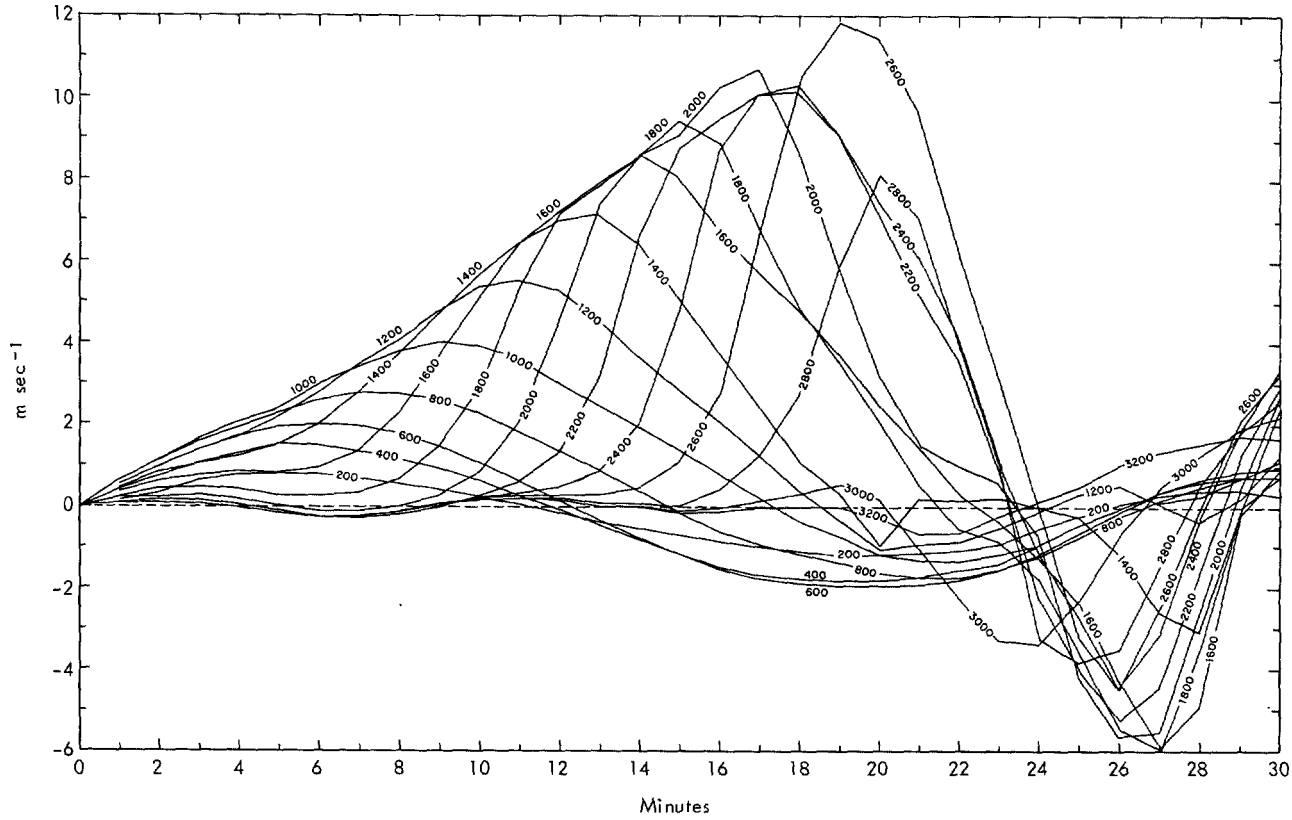

FIGURE 3.—Vertical wind component for several levels on the central axis, case A.

stage, but case D subsequently showed collapse of the cloud and updraft, followed by total evaporation and eventual regeneration of the cloud. This evolution is of little interest, however, because of the unnatural conditions arising from the proximity of the cloud to the upper boundary, which acts somewhat like an infinitely strong inversion.

The two cases with shallow impulse showed a much more moderate development, with maximum updraft of 12 m s^{-1} in both cases, and a cloud top of 3 km for case A and 3.6 km for case C. The cloud-top heights were reasonable for trade cumuli, and the updrafts not too excessive. The liquid water content [1] at the time of maximum was between two and three times as much for B and D as for A and C. By comparison, the impulses for B and D added nearly an order of magnitude more water than those for A and C.

It appears that the size of the simulated cloud and the strength of its updraft are strongly dependent on the depth of the initial humidity impulse. In a general way, this is consistent with the observation by Malkus (1958) that the areas of greater cloudiness are characterized by deeper mixed layers, which is to say, deeper layers of high humidity.

The total amount of water added by the impulse is not the sole controlling agent on the rate and amount of

[1] Cloud physicists use liquid water content, which is mass per unit volume. In dynamic models, it is more convenient to use mixing ratio, which is mass of water per mass of dry air. In the lower atmosphere, liquid water content in grams per cubic meter approximates mixing ratio in grams per kilogram.

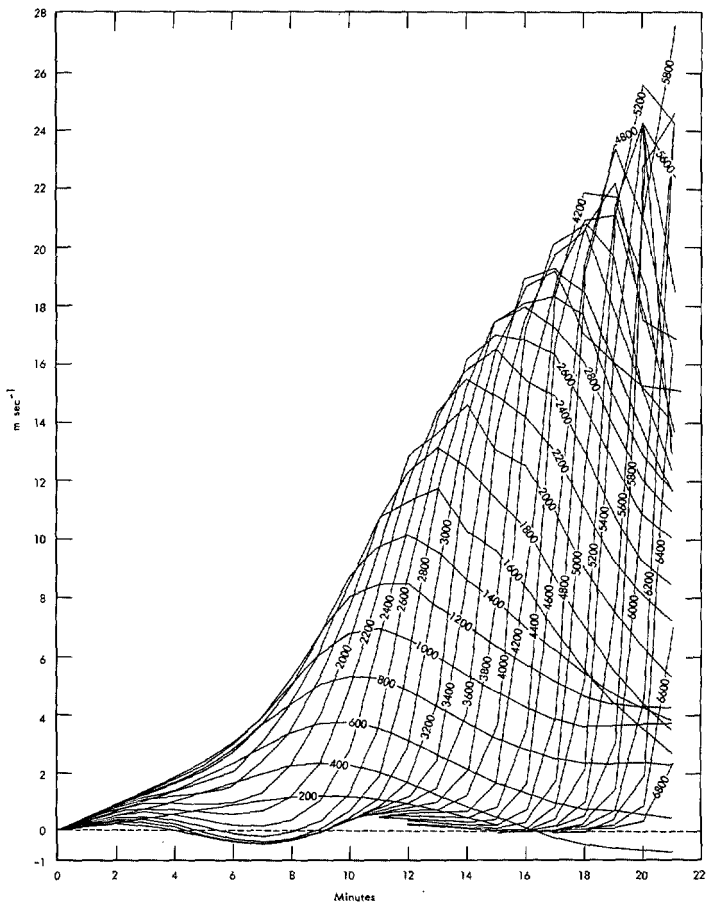

FIGURE 4.—Same as figure 3, except for case B.

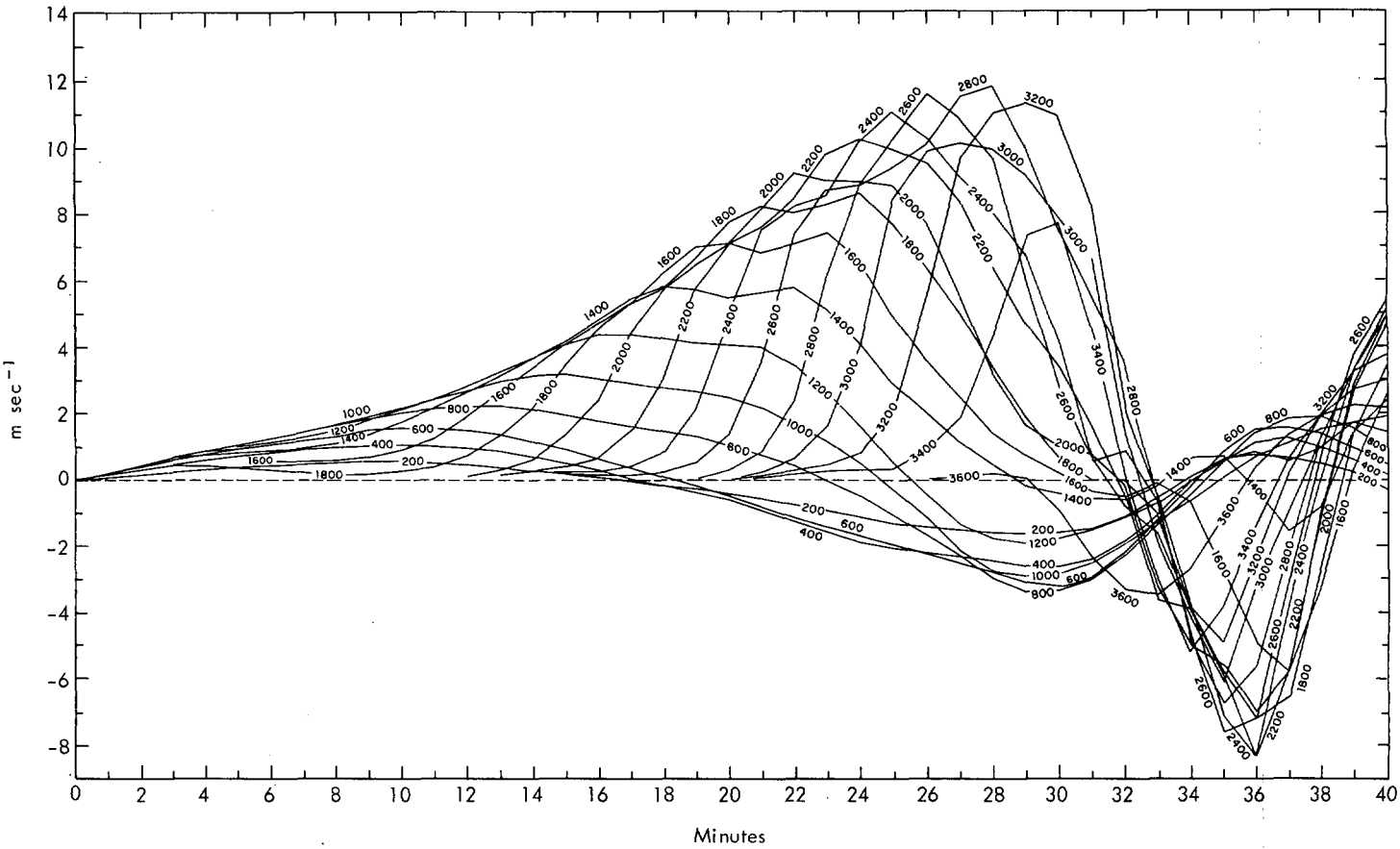

FIGURE 5.—Same as figure 3, except for case C.

development. For instance, case C started with four times the added water of case A, but its maximum height was only 600 m greater, its maximum mixing ratio of liquid water 1 g kg^{-1} greater, and its maximum updraft the same; whereas it took 6 to 8 min longer to attain these values. The difference between the two cases lies in the width of the impulse; and though the wider impulse resulted in a larger and wetter cloud, the narrower impulse led to faster growth. Much the same conclusions can be had by examination of cases B and D, but the situation is less clearcut because the clouds reached the upper boundary.

The effect of impulse width on cloud size is in agreement with ideas derived from the theory of entrainment. One-dimensional models that treat entrainment explicitly, such as that of Simpson and Wiggert (1969), show this effect very clearly. The present model does not treat entrainment explicitly, but entrainment occurs in it in two ways. One way is through the eddy-diffusion term; this is dependent on the value of the coefficient selected. The other is through the Lagrangian technique used for computing temperature and moisture. If, for example, a single-time-step trajectory ending at a grid point with nonzero liquid water starts in a grid square with one or more vertices outside the cloud, the advection effect will tend to decrease the liquid water content at the terminal grid point, and

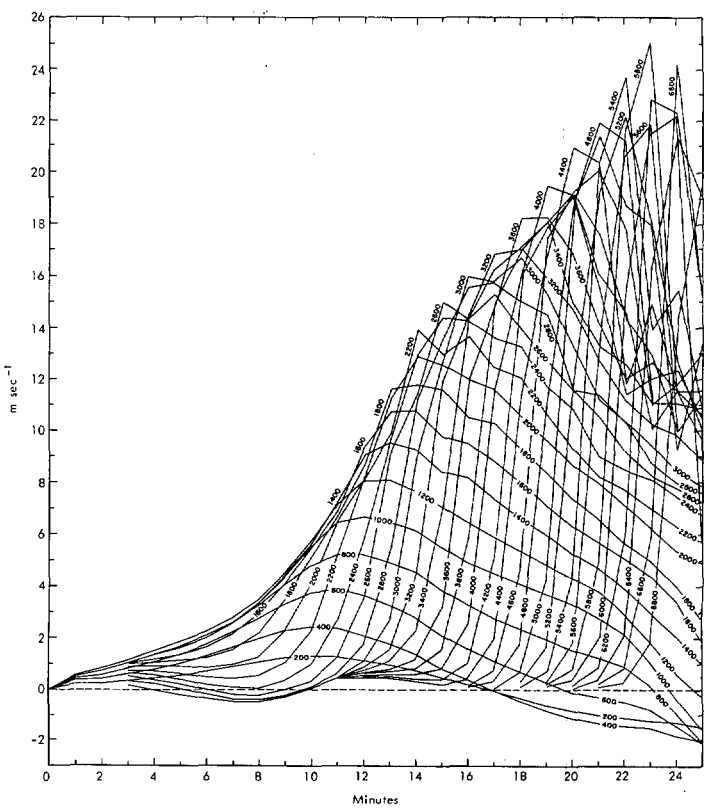

FIGURE 6.—Same as figure 3, except for case D.

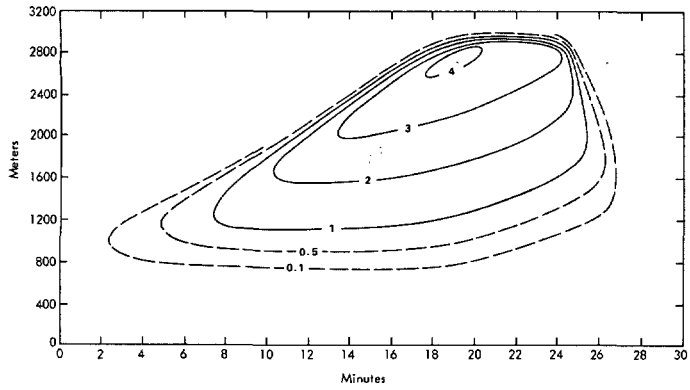

FIGURE 7.—Time section of mixing ratio of liquid (g kg^{-1}), case A.

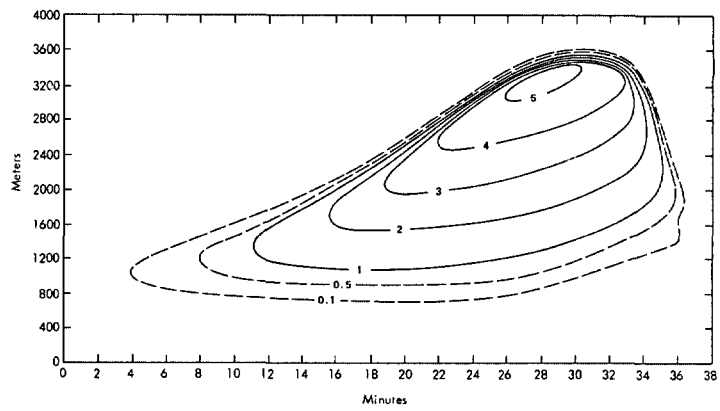

FIGURE 9.—Same as figure 7, except for case C.

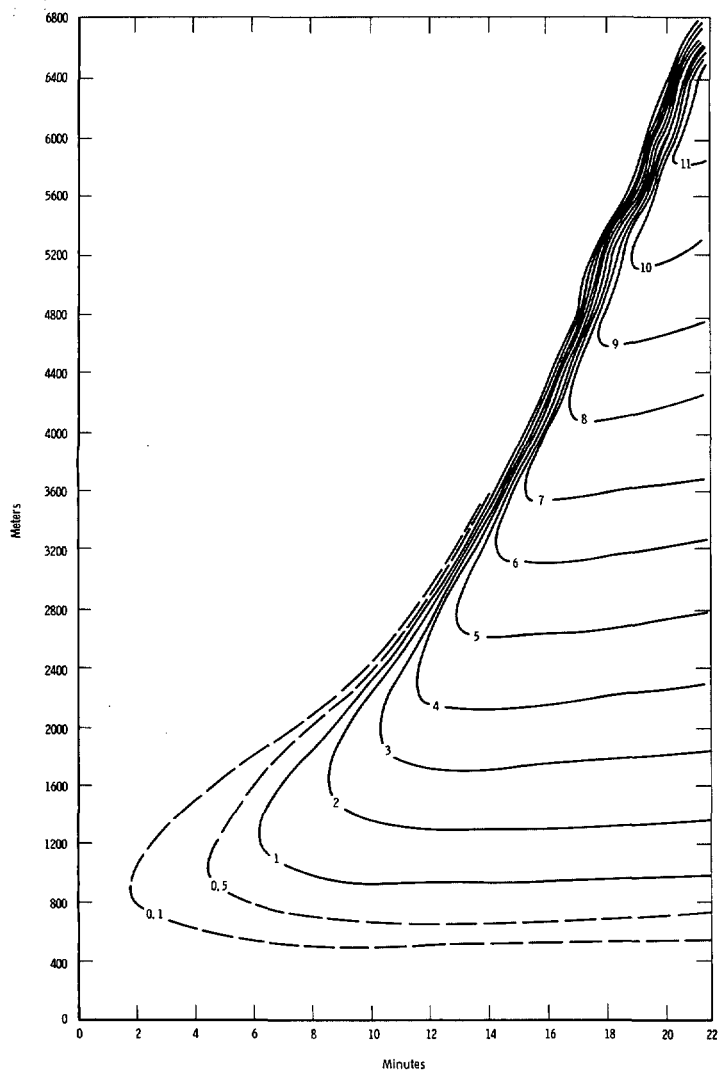

FIGURE 8.—Same as figure 7, except for case B.

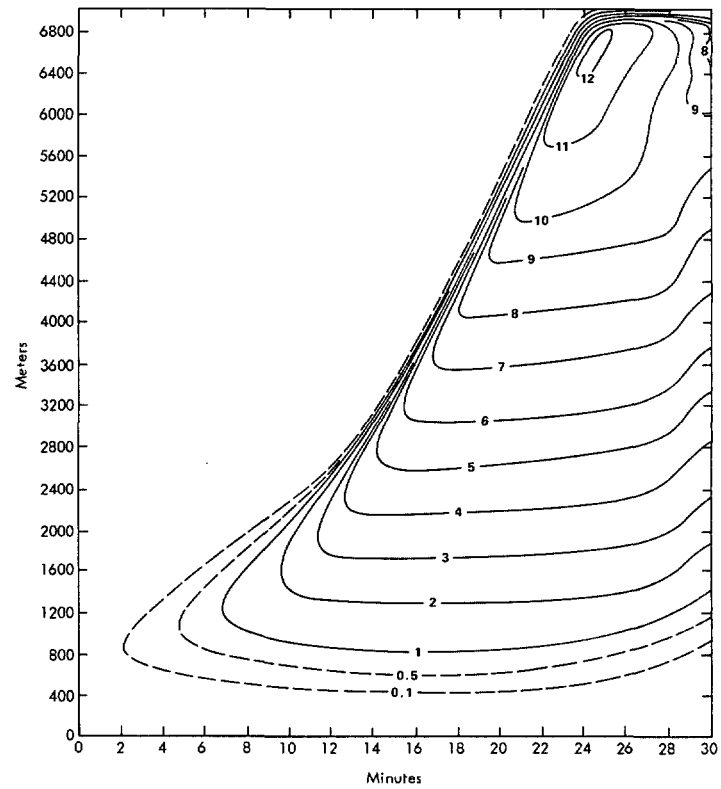

FIGURE 10.—Same as figure 7, except for case D.

similarly for water vapor and temperature departure. This effect cannot readily be altered in the model; but if it should be determined that the model is deficient in entrainment, the eddy-diffusion coefficient can easily be increased.

An interesting feature of figures 3–6 is the way they demonstrate how the level of maximum wind rises. At any given height, there is a peak value at the time when the main cloud vortex is passing through that height, with rapid acceleration before that time and rapid deceleration afterward. Comparison of figure 3 with 7, figure 4 with 8, etc., shows that the time of maximum updraft at a given height is connected closely with the time at which the liquid water reaches its maximum at that height. Both the rate at which the updraft increases to its maximum and the magnitude of the maximum increase with height, reflecting the acceleration of the rise of the vortex.

In real clouds, the center of the vortex cannot be observed readily, but the cloud top can. Figures 7–10 enable us to study the rise of the "visible" top of the simulated cloud. It is seen that, for case A (fig. 7), the cloud top ascended at about 2.2 m s^{-1}, leveling off near 3 km at 20 min. The rate of ascent of the cloud top was fairly uniform from 3 to

17 min while the maximum updraft varied from 1.5 to 10.5 m s^{-1}, averaging 6 m s^{-1}. A rule of thumb from observation is that the cloud rises at half the speed of the maximum updraft, so the figures in this case seem to be reasonable. The cloud base held steady just below 800 m during the growing stage and then started to rise as dissipation commenced. At middle levels within the cloud, the slow decrease in the amount of liquid water probably represents entrainment of drier air through turbulent diffusion. The maximum value of 4 g kg^{-1} is quite reasonable.

By contrast, figure 8 shows that the cloud top of case B rose at 2.8 m s^{-1} during the first 10 min and 9.1 m s^{-1} during the last 10. The water content reached an unrealistic 11.6 g kg^{-1}, there being no precipitation mechanism in the model. The maximum updraft averaged about 4 m s^{-1} during the first 10 min and about 19 m s^{-1} during the last 10 min, still in agreement with the rule of thumb. However, even though the ratio of rate of cloud rise to updraft is reasonable, the magnitudes are not.

Comparison of figure 3 with 5 and figure 7 with 9 shows that the rate of development was less for case C than for case A, though the eventual amount of development was greater. On the other hand, figures 4 and 6 show that the updraft in case B increased faster and had a larger maximum than in case D. Figures 8 and 10 show that condensation proceeded more rapidly in case B, but the eventual maximum value of liquid water content is not subject to comparison because of the cloud's reaching the upper boundary. These results suggest that, for a given impulse depth, the wider impulse leads to a taller, wetter cloud. However, the narrower impulse leads to more rapid development, particularly of the updraft; this is perhaps a consequence of the built-in convergence of the cylindrical coordinate system. Also, the narrower impulse has a stronger gradient of atmospheric density because the same total change occurs over a shorter distance.

The evolution of the radius of the simulated clouds is shown in figure 11. In all cases, there was rapid growth during the first 4 min (organization stage) to a value that tends to be somewhat less than half the total width of the initial impulse. Since cases B and C stabilized at the same width, we conclude that impulse width dominates rather than impulse depth or total water added. However, while the cloud was still rising rapidly and the updraft still increasing, the cloud width started to diminish. The converse frequently happens in real clouds, so the mechanisms of the model should be examined in this respect. Murray (1970) has noted that, though the axisymmetric model has relatively small downdrafts as compared with the updrafts, the downdrafts are concentrated near the outer edge of the simulated cloud, leaving most of the computational region with extremely slow vertical motion. The vertical boundary between updraft and downdraft tends to lie within the vertical boundary between liquid and no liquid, that is, within the cloud. Thus, the outermost part of the cloud is subject to evaporation, particularly while the circulation is at maximum strength. In terms of entrainment, it is seen that the dynamics of the model produce an envelope about the most active region of the cloud, consisting of air that has been dried by subsidence. Entrainment of this air dilutes the cloud more than would entrainment of air from the undisturbed environment.

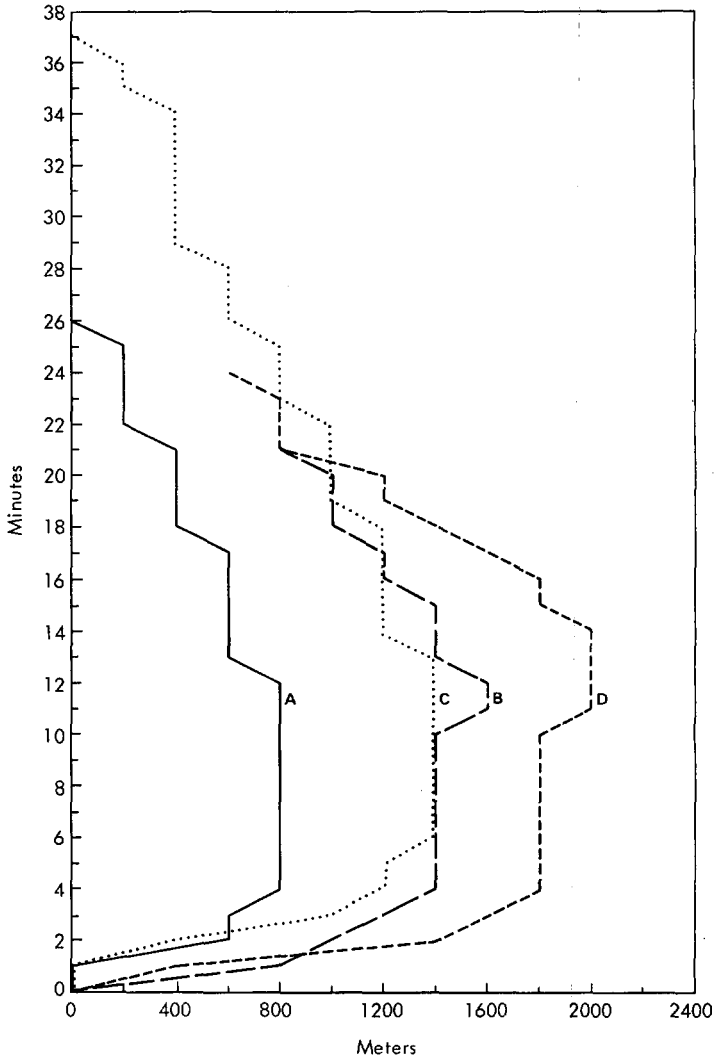

FIGURE 11.—Maximum cloud radius versus time, four cases.

The ultimate effect of the eddy exchange mechanism is not entirely clear in this situation. Near the cloud edge, it brings drier air into the cloud, and it also moves liquid water out to where it can be evaporated. On the other hand, it also transports water from the center of the cloud, where the liquid water content is highest, out toward the edges, where it can counteract the dilution. Where the circulation is not strong, the eddy diffusion tends to spread the cloud; but with a vigorous downdraft near the cloud edge, the net result may be the opposite.

An interesting detail is that, shortly before the shrinkage started, both deep-impulse cases showed a slight temporary expansion. The subsequent shrinkage for case D was exceptionally rapid, even while the cloud was approaching the upper boundary. As a matter of fact, for several minutes after reaching that boundary, the width of the upper part of the cloud stayed at 600 m and then dropped to 400 m, following which the cloud expanded a little in its *lower* part. This is not entered in figure 11.

From figures 3 and 5, it can be seen that, shortly after the updraft associated with the shallow impulse reached

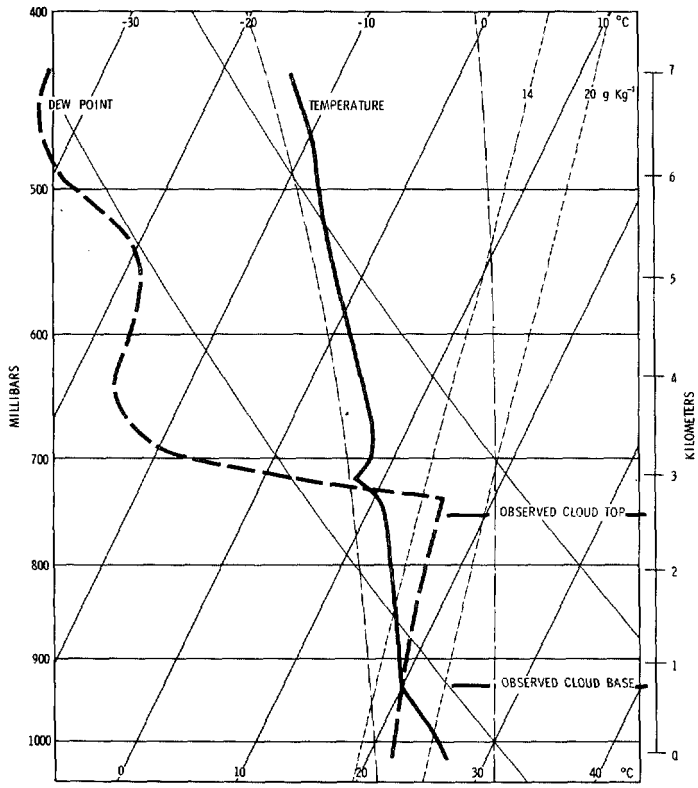

FIGURE 12.—Computed sounding at 19 min, on axis, case A, San Juan, Puerto Rico, at 1200 GMT on July 17, 1967.

its maximum value, it diminished very rapidly and gave way to a downdraft. At 24 min for case A and 33 min for case C, the vertical component of wind on the central axis was directed downward at all levels. Thereafter, an oscillation occurred, but with small amplitude.

Concurrently with the onset of the downdraft, the clouds started dissipating by evaporation; see figures 7 and 9. Within a very few minutes, they vanished entirely and did not reappear even though the computation was continued out to about 60 min. The dissipation of the cloud was very abrupt, occurring almost simultaneously at all levels.

4. COMPARISON WITH OBSERVATIONS

The basic sounding (San Juan, Puerto Rico, at 1200 GMT on July 17, 1967) was chosen because on that and the following day the Naval Research Laboratory was flying instrumented aircraft in and around clouds in the vicinity. Case A was selected for comparison because it had the smallest perturbation.

As the variables change in the course of the computation, it is possible to read out computed soundings along any vertical at any time. At 19 min of simulated time, the cloud had reached its peak of development. The computed sounding along the central axis at this time is shown in figure 12; it shows the characteristics that one might deduce by applying the parcel method to the initial sounding (fig. 1). In particular, below the condensation level, the lapse rate has become nearly dry-adiabatic; within the cloud, it is very close to the saturation adiabatic; and from the ground surface nearly to the top of the simulated cloud, the mixing ratio of total water is constant. (In figs. 12 and 13, the evaporation dew point is plotted where liquid water exists; see the appendix.) The simulated cloud is only a little deeper than typical clouds observed on that day. At the top of the simulated cloud, the sounding shows the cold cap invariably found in these computations and presumably found in nature as well. This phenomenon results mainly from forced lifting and consequent dry-adiabatic cooling of the air immediately above the level of the cloud but also from evaporation in the topmost layer. In cases where there is a large temperature excess within the cloud, a superadiabatic lapse rate may be found over one or two mesh units; but in the present instance, the lapse rate is less steep. This can be attributed to the fact that the initial lapse rate is close to the saturated adiabatic, so little excess temperature can be developed. At higher levels, the computed sounding differs slightly from the initial sounding.

Das (1969) has pointed out that the lapse rates seen in figure 12 are the result of the assumption that condensation or evaporation will lead to exact saturation; whereas when drop size is taken into consideration, this will not necessarily be the case. Another reason for the close agreement between the computed sounding on the central axis and the results of the parcel method is that the absence of a horizontal component of motion on the central axis precludes dynamic entrainment. Turbulent entrainment occurs through the eddy-diffusion term, but its magnitude is small. Away from the central axis, however, dynamic entrainment can be of major importance. This is illustrated by figure 13 showing the computed soundings 200 and 600 m from the central axis. The first is within the cloud, but it bears significant differences from that of figure 12. The temperature within the cloud is noticeably cooler, and the cold cap is lower and a little less pronounced. The main difference, however, is in the humidity curve, which is well to the dry side of that of figure 12 and which shows a decrease with height up to a point near the center of the cloud.

The computed sounding along a vertical outside the cloud, 600 m from the axis, is quite different. In the lower levels, it shows considerable warming; but it, too, shows an effect of the cold cap. The cold air above the cloud is carried outward and downward by the circulation, and it shows distinctly on the clear-air sounding. Incidentally, the upper part of the sounding, just below the cold cap, shows remarkable agreement with an aircraft sounding made during the afternoon 40 mi south of Ponce. The dew-point curve shows fair agreement in its general shape, particularly at low levels and near the cloud top. However, in the cloud layer, the observation shows drier air than the computation.

Aircraft made several traverses just beneath the cloud base, yielding a limited opportunity for comparison of computation with observation. Temperature and dew-point profiles below a cloud similar in height and width to that of case A are shown in figure 14 together with the corresponding computed profiles. Observed values were not symmetric about the central axis of the cloud; the plotted data are from the half during which the aircraft

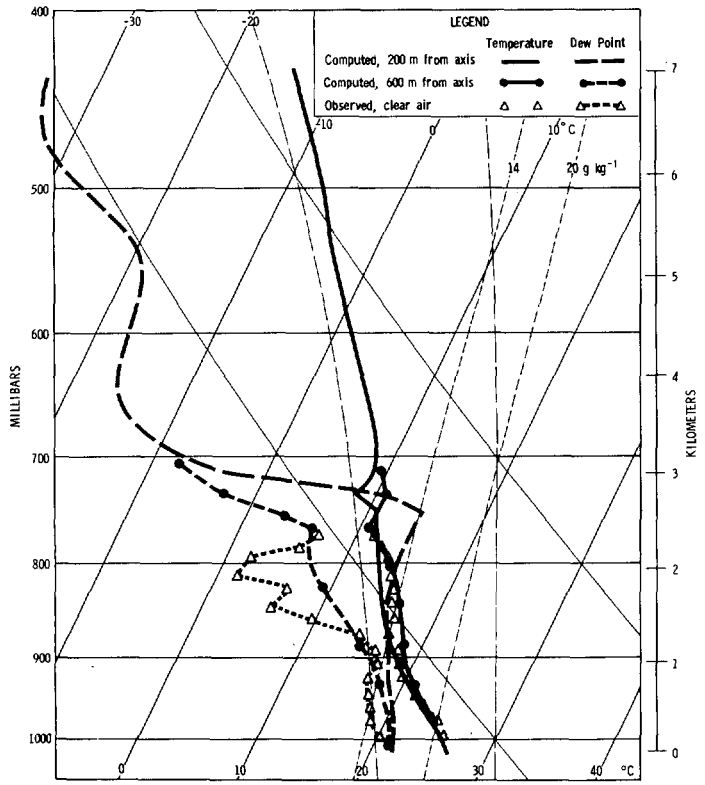

FIGURE 13.—Computed sounding at 19 min, off axis, case A, San Juan, Puerto Rico, at 1200 GMT on July 17, 1967. The observations at 1700 GMT are 40 mi south of Ponce, Puerto Rico.

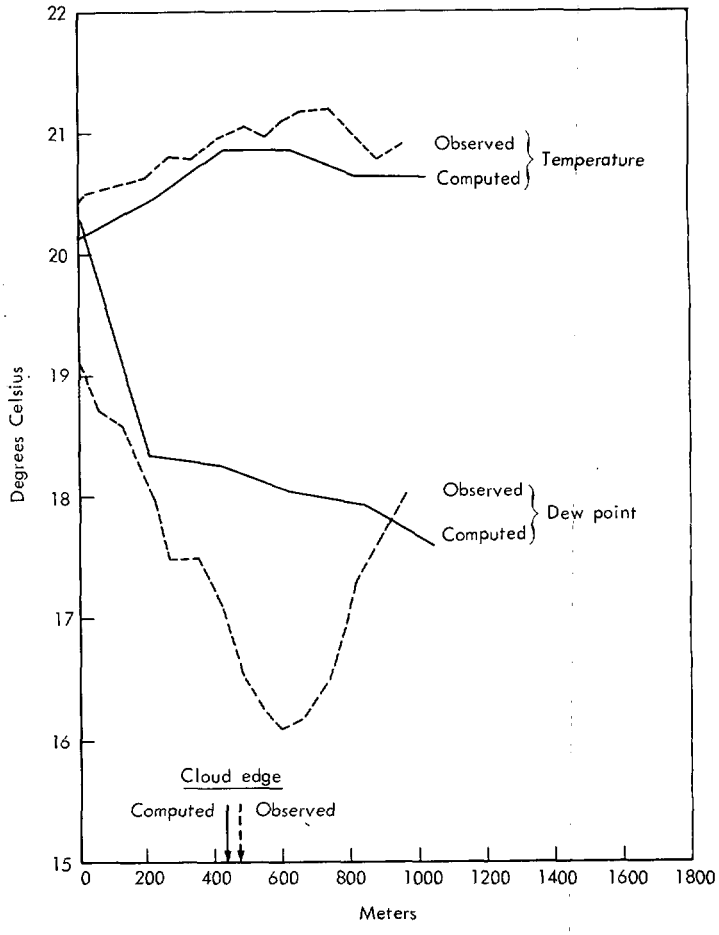

FIGURE 14.—Temperature and dew point immediately below cloud base.

was moving away from the axis. Even though there was a degree of selection of data for best fit, the correspondence between computation and observation is not impressive, especially regarding the dew point. The two temperature profiles do remain within a few tenths of a degree of each other and have the same trend—coldest at the central axis and warmest a few hundred meters beyond the cloud edge. This reflects the warming of the downdraft just outside the cloud and illustrates a reason for the frequently noted reverse-circulation cell below the simulated cloud. The dew-point curves show a progressive drying with distance from the central axis, but the observed curve reaches strong minimum less than 200 m beyond the cloud edge and then recovers sharply; whereas the computed one continues its decline, but at a moderate rate. This suggests that a computed sounding farther from the axis than 600 m might have a dew-point curve more comparable to the observed curve of figure 13 than the one shown. As a matter of fact, a computed sounding at 1200 m (not illustrated) does show lower dew points, more in keeping with the observations plotted in figure 13.

Unfortunately, data are not available from aircraft penetrations of clouds on the day of this experiment, but some are for the following day, on which the basic sounding was virtually unchanged. They indicate that the amount of liquid water present in the simulated cloud is realistic, but slightly high. This is explained easily by the absence of a precipitation mechanism in the simulated cloud. Even if the cloud did not develop to the rain stage, gravitational settling of liquid water would diminish the value in the upper parts of the cloud, perhaps increase it in the lower parts, and cause further cooling below the cloud by evaporation.

The radius and thickness of several clouds investigated by Naval Research Laboratory aircraft on July 17 and 18 are shown in figure 15. Two least-squares curves computed from the observed values are shown in the figure, one to predict thickness from radius and one to predict radius from thickness. One should not place much confidence in results from such a small (and perhaps biased) sample, but it is interesting to note that the corresponding values from cases A and C fit the observations quite well. (Note that computed radius is taken from fig. 11 and so is somewhat less than the radius of the initial impulse.) It is a plausible supposition that, with additional experience with the model in connection with observed clouds, the impulse can be "tuned" so as to achieve consistently results in forecasting maximum cloud thickness comparable to the excellent results reported by Simpson et al. (1967) and Simpson and Wiggert (1969) for a one-dimensional model.

These few items of correspondence between computation and observation are admittedly inadequate, offering little but the assurance that the computational results are not wildly improbable. But the difficulties in obtaining suitable observational data are formidable indeed.

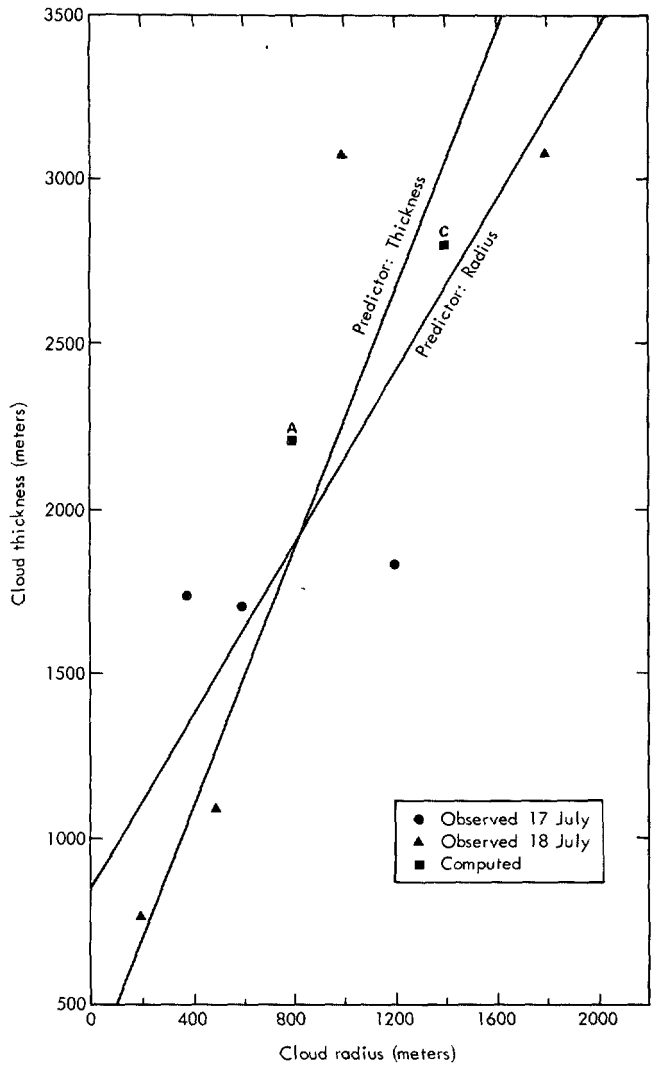

FIGURE 15.—Relationship between cloud radius and cloud thickness for several observed clouds and for cases A and C. The diagonals are the least-squares fittings of the observations.

It is very expensive to mount an expedition to measure clouds; and even for such a quantity as liquid water content, different types of sensors frequently give widely differing values. Another problem arises from the relatively short life cycle of a cumulus cloud. The computed clouds vary from nothing at initial time through a state of vigorous development to a state of decay in simulated time of less than an hour, and the same can be said of a natural cumulus cloud. But whereas the instantaneous state of development of a simulated cloud can be determined with relative ease, this is not true of a natural cloud. It is frequently difficult to determine just which time step of a cloud simulation to use in making comparisons with observations of a real cloud.

Despite these difficulties, it has been possible to make a number of interesting comparisons of observations with simulated clouds. On the whole, these comparisons have led to the belief that the present numerical model is a reasonably good approximation to actual cumulus convection and that further experimentation with it and refinement of it are desirable.

5. SUMMARY AND CONCLUSIONS

Earlier work in the numerical simulation of cumulus clouds, both by the author and by others, has almost invariably used local warming as the initial impulse to start the convection. That procedure, however, has certain shortcomings; and so on the basis of theory and some observational evidence, the present experiment in the use of a humidity impulse was undertaken.

It was determined that the vigor of the subsequent development of the simulated cloud is closely related to the depth of the humidity impulse. Where the impulse is shallow, the cloud grows slowly, eventually attaining maximum height and maximum updraft speed at reasonable values and then entering the decaying stage. With the deep impulse, however, the updraft becomes excessively strong, the cloud top rises to a disquieting proximity to the upper boundary of the computational region, and the liquid-water content becomes exceedingly high. The deep perturbation adds a great deal more water vapor to the system than does the shallow one, and this water vapor becomes a source of energy for the subsequent development. Such deep perturbations, however, are not at all realistic. On the basis of the present and previous work (Murray 1970), it is suggested that the humidity impulse should be confined to the rather shallow transition layer near the lifting condensation level.

The rationale of the humidity impulse is as follows: In accordance with the observations of Bunker et al. (1949) and Malkus (1958), the tropical maritime atmosphere in relatively clear areas has a mixed layer some 600 m in depth, surmounted by a transition layer 200 m in depth surmounted by a drier but still relatively moist layer extending up to the trade inversion near 2000 m. Cloudy areas differ mainly by having a deeper mixed layer, moister near its top, and little or no transition layer. This suggests a horizontal variation in humidity that is most pronounced near the lifting condensation level. These generalizations are valid over horizontal distances of 20 to 30 km. In the model, it is assumed that the same type of variation can occur over 2 or 3 km, and there is some confirmation for this assumption in the observations. In the four cases discussed here, there was too great an attempt to make the initial vertical profile at the center of the perturbation conform with the idealized cloudy-area sounding, resulting in initial horizontal humidity gradients over rather deep layers, contrary to observations. The outcome, especially in cases B and D, was excessively rapid growth. However, with a more realistic shallow impulse, the simulated cloud corresponds reasonably well to observed clouds.

In one-dimensional models where an entrainment law is assumed such that rate of entrainment decreases with increasing cloud mass (e.g., Simpson and Wiggert 1969),

the subsequent height attained by a simulated cloud is directly controlled by the assumed cloud radius; that is, a wide cloud base leads to a tall cloud. This is a direct outcome of the parcel method modified by progressive dilution of the parcel. Excellent forecasts of cloud height have been obtained with this type of model.

The two-dimensional model, however, does not have such a simple relationship. It is true that the narrow impulse of case A led to a cloud of modest depth and the wide impulses of cases B and D led to tall, wide clouds. However, the equally wide impulse of case C led to a cloud only slightly deeper than the cloud of case A. It is apparent that, in these cases, the cloud depth is more dependent on impulse depth than on impulse width. If, however, the impulse is kept realistically shallow, cloud height and width vary together, as expected. Very limited observations suggest that the magnitude of this variation is about right.

The tendency of the two-dimensional model cloud to shrink in width during its period of most vigorous growth is troublesome. This comes about because of the strong downdraft just outside the cloud, which of course cannot exist in a one-dimensional model cloud. It would appear that the two-dimensional model has too much entrainment in this situation. Experiments in progress suggest that the problem may be alleviated by more elaborate treatment of the microphysics to include some liquid water in the form of large drops that do not evaporate as quickly as the small cloud drops.

The two-dimensional model with a humidity impulse has produced simulated clouds that agreed in many respects with clouds observed in nature. Provided the energy added to the system was kept sufficiently small by restricting the depth of the impulse, the humidity impulse has proved more satisfactory than the more commonly used temperature impulse.

APPENDIX—EVAPORATION DEW POINT

In plotting soundings through an atmosphere in which liquid water may be present, it is advantageous to have a variable that represents the total water, both liquid and vapor. The evaporation dew point is such a variable, and a particularly useful one, for it is easily plotted on a thermodynamic diagram, graphically shows the depth of the cloud, and, moreover, can be directly measured with airborne equipment (Ruskin 1967).

The numerical model described in this report carries moisture values in the form of mixing ratio. Thus q_v is the mass of water vapor per unit mass of dry air, and q_l is the mass of liquid water per unit mass of dry air. It is desirable to express both ordinary and evaporation dew point in terms of these variables.

The saturation vapor pressure is given by

$$e_s=e_0 \exp\left\{\frac{a(T-273.16)}{T-b}\right\} \tag{1}$$

where T is temperature in degrees Kelvin and

$$e_0=6.1078,$$
$$a=17.2693882, \text{ and}$$
$$b=35.86$$

for saturation over water (Murray 1967).

If eq (1) is solved for T, one obtains

$$T=\frac{273.16\,a-b\ln\frac{e_s}{e_0}}{a-\ln\frac{e_s}{e_0}}. \tag{2}$$

The dew point of a parcel of air not containing liquid water is defined as the temperature the parcel would have if cooled isobarically until it is saturated. Thus, if a parcel had vapor pressure e, its dew point T_d would be found by substituting e for e_s and T_d for T in eq (2), or

$$T_d=\frac{273.16\,a-b\ln\frac{e}{e_0}}{a-\ln\frac{e}{e_0}}. \tag{3}$$

The vapor pressure is related to the mixing ratio through

$$q_v=\frac{\epsilon e}{p-e};\quad e=\frac{pq_v}{q_v+\epsilon} \tag{4}$$

where p is the total pressure and $\epsilon=0.622$ is the ratio of molecular weights of water vapor and air. Combination of eq (3) and (4) yields

$$T_d=\frac{273.16\ a-b\ln\left\{\frac{p}{e_0}\frac{q_v}{(q_v+\epsilon)}\right\}}{a-\ln\left\{\frac{e}{e_0}\frac{q_v}{(q_v+\epsilon)}\right\}}. \tag{5}$$

If liquid water or ice is present, the evaporation dew point is defined as the ordinary dew point that the parcel would have if all of the liquid and ice were evaporated. Since presumably a parcel containing liquid water or ice is already at the point of saturation, evaporation into it requires an increase of saturation vapor pressure, and consequently through eq (2) an increase of temperature. Therefore, whereas the ordinary dew point is never greater than the temperature (barring supersaturation), the evaporation dew point is always greater than the temperature unless there is no liquid or ice present, in which case the two dew points are identical.

Let the total mixing ratio be the sum of the mixing ratios of vapor, liquid, and ice; or

$$q=q_v+q_l+q_i. \tag{6}$$

If all the liquid and ice were evaporated, the value of q would be unchanged, but it would now represent the mixing ratio of vapor; that is, q_v would increase by the amount that q_l+q_i decreased in going to zero. Hence, by

comparison with eq (5), the evaporation dew point is given by

$$T_e=\frac{273.16\,a-b\ln\left\{\frac{p}{e_0}\frac{q}{(q+\epsilon)}\right\}}{a-\ln\left\{\frac{p}{e_0}\frac{q}{(q+\epsilon)}\right\}}. \quad (7)$$

Obviously, when $q_l+q_i=0$, eq (5) and (7) are identical, and $T_d=T_e$.

When soundings were computed for the present report, the dew point was found from eq (7) with $q_i\equiv 0$. Where the curve of T_e is to the left of the curve of T on the thermodynamic diagams, $T_d=T_e$. Where the curve of T_e is to the right of the curve of T, it is assumed that $T_d=T$. In this case, the difference between the curves of T_e and T, read on the mixing-ratio scale of the diagram, represents the liquid water.

ACKNOWLEDGMENTS

This research was supported by the Office of Naval Research under Contract No. N00014-67-C-0101, Requisition 00178-6-006280, and by the Navy Weather Research Facility under Contract No. N62306-69-C-0408.

Thanks are gratefully extended to J. E. Dinger and R. E. Ruskin of the Naval Research Laboratory for making available results of their field observations of tropical cumuli. Numerous helpful suggestions were made by Joanne Simpson of the NOAA Experimental Meteorology Laboratory, for which appreciation is expressed.

REFERENCES

Bunker, Andrew F., Malkus, Joanne S., Haurwitz, Bernhard, and Stommel, H., "Vertical Distribution of Temperature and Humidity Over the Caribbean Sea," *Papers in Physical Oceanography and Meteorology*, Vol. 11, No. 1, Massachusetts Institute of Technology and Woods Hole Oceanographic Institution, **1949**, 82 pp.

Das, Phanindramohan, "The Thermodynamic Equation in Cumulus Dynamics," *Journal of the Atmospheric Sciences*, Vol. 26, No. 3, May **1969**, pp. 399–407.

Langwell, Patricia A., "Inhomogeneities of Turbulence, Temperature, and Moisture in the West Indies Trade Wind Region," *Journal of Meteorology*, Vol. 5, No. 5, Oct. **1948**, pp. 243–246.

Lilly, Douglas K., "On the Numerical Simulation of Buoyant Convection," *Tellus*, Vol. 14, No. 2, May **1962**, pp. 148–172.

Malkus, Joanne S., "On the Structure of the Trade Wind Moist Layer," *Papers in Physical Oceanography and Meteorology*, Vol. 13, No. 2, Massachusetts Institute of Technology and Woods Hole Oceanographic Institution, **1958**, 47 pp.

Malkus, Joanne S., and Witt G., "The Evolution of a Convective Element: A Numerical Calculation," *The Atmosphere and the Sea in Motion*, Rockefeller Institute Press, New York, **1959**, pp. 425–439.

Murray, F. W., "On the Computation of Saturation Vapor Pressure," *Journal of Applied Meteorology*, Vol. 6, No. 1, Feb. **1967**, pp. 203–204.

Murray, F. W., "Numerical Models of a Tropical Cumulus Cloud With Bilateral and Axial Symmetry," *Monthly Weather Review*, Vol. 98, No. 1, Jan. **1970**, pp. 14–28.

Murray, F. W., and Anderson, C. E., "Numerical Simulation of the Evolution of Cumulus Towers," *Report* SM-49230, Douglas Aircraft Company, Inc., Santa Monica, Calif., Oct. **1965**, 97 pp.

Ogura, Y., "The Evolution of a Moist Convective Element in a Shallow, Conditionally Unstable Atmosphere: A Numerical Calculation," *Journal of the Atmospheric Sciences*, Vol. 20, No. 5, Sept. **1963**, pp. 407–424.

Orville, H. D., "Ambient Wind Effects on the Initiation and Development of Cumulus Clouds Over Mountains," *Journal of the Atmospheric Sciences*, Vol. 25, No. 3, May **1968**, pp. 385–403.

Ruskin, R. E., "Measurements of Water-Ice Budget Changes at −5C in AgI Seeded Tropical Cumulus," *Journal of Applied Meteorology*, Vol. 6, No. 1, Feb. **1967**, pp. 72–81.

Simpson, Joanne, and Wiggert, Victor, "Models of Precipitating Cumulus Towers," *Monthly Weather Review*, Vol. 97, No. 7, July **1969**, pp. 471–489.

Simpson, Joanne, Brier, Glenn W., and Simpson, Robert H., "Stormfury Cumulus Seeding Experiment 1965: Statistical Analysis and Main Results," *Journal of the Atmospheric Sciences*, Vol. 24, No. 5, Sept. **1967**, pp. 508–521.

Vul'fson, N. I., "Effect of Air Humidity on Development of Convection in a Cloudless Atmosphere" (Vliyaniye vlazhnosti vozdukha na razvitiye konvektivnykh divzheniy v bezoblachnoy atmosfere, July–Aug. 1963), *Doklady Academiia Nauk SSSR, Earth Science Sections, Vol. 151, July–Aug. 1963* (Translation), American Geological Institute, Washington, D.C., Mar. **1964**, pp. 10–12.

[*Received November 24, 1969; revised June 25, 1970*]